**You might find this additional information useful...**

This article cites 33 articles, 12 of which you can access free at:
http://jn.physiology.org/cgi/content/full/96/3/1237#BIBL

Updated information and services including high-resolution figures, can be found at:
http://jn.physiology.org/cgi/content/full/96/3/1237

Additional material and information about *Journal of Neurophysiology* can be found at:
http://www.the-aps.org/publications/jn

This information is current as of June 8, 2010 .

# Metabolic Energy Cost of Action Potential Velocity

**Patrick Crotty,[1] Thomas Sangrey,[3] and William B Levy[1,2]**
[1]*Department of Neurological Surgery, University of Virginia Health System and* [2]*Department of Psychology, University of Virginia, Charlottesville, Virginia; and* [3]*Department of Biology, Emory University, Atlanta, Georgia*

Crotty, Patrick, Thomas Sangrey, and William B Levy. Metabolic energy cost of action potential velocity. *J Neurophysiol* 96: 1237–1246, 2006. First published March 22, 2006; doi:10.1152/jn.01204.2005. The action potential of the unmyelinated nerve is metabolically expensive. Using the energetic cost per unit length for the biophysically modeled action potential of the squid giant axon, we analyze this cost and identify one possible optimization. The energetic cost arising from an action potential is divided into three separate components: *1*) the depolarization of the rising phase; *2*) the hyperpolarization of the falling phase; and *3*) the largest component, the overlapping of positive and negative currents, which has no electrical effect. Using both the Hodgkin–Huxley (HH) model and an improved version of the HH model (HHSFL), we investigate the variation of these three components as a function of easily evolvable parameters, axon diameter and ion channel densities. Assuming conduction velocity is well designed for each organism, the energy component associated with the rising phase attains a minimum near the biological values of the diameter and channel densities. This optimization is explained by the membrane capacitance per unit length. The functional capacitance is the sum of the intrinsic membrane capacitance and the gating capacitance associated with the sodium channel, and this capacitance minimizes at nearly the same values of diameter and channel density. Because capacitance is temperature independent and because this result is independent of the assumed velocity, the result generalizes to unmyelinated mammalian axons. That is, channel density is arguably an evolved property that goes hand-in-hand with the evolutionary stability of the sodium channel.

## INTRODUCTION

In the nervous system, the action potential is used for long-distance information transmission. Delivery of such information in a timely fashion requires an action potential of sufficient velocity. On the other hand, sufficient velocity has its costs. In what follows, we assume that across species and across the life span of the organism the velocity of any axon is appropriate to its role in information processing.

In the neuropil of neocortex, where axons must be unmyelinated if each one is to make several thousand sequential or neighboring synapses, the metabolic costs are surprisingly large. Attwell and Laughlin (2001) estimated that 75% of the adenosine triphosphate (ATP) consumed by neurons in the rat brain is used for communication and computation. Of this, half is used by the unmyelinated axons.

This metabolic perspective contrasts with and, as we will see, ultimately complements Hodgkin's conjectured constraint on action potential velocity. Both Hodgkin (1975) and Adrian (1975) proposed that the gating charge movement that inevitably accompanies rapid activation of a voltage-dependent

channel leads to an optimal density of fast $Na^+$ channels. This optimization occurs because the movement of charge specifically restricted to the transmembrane voltage field contributes, albeit transiently, to membrane capacitance. Because increasing capacitance slows action potential propagation, Hodgkin proposed that the $Na^+$ channel density has evolved to maximize velocity. Unfortunately, biophysical parameter sweeps do not support this conjecture (Sangrey et al. 2004). In a simple Hodgkin–Huxley model reparameterized to fit the action potential velocity with high precision, the conjecture misses by twofold. When a more sophisticated model, i.e., one that takes into account that as many as six equivalent charges move across the membrane but are only sequentially available, the conjecture fails with more than a fourfold error.

Here we combine the gating-charge-as-capacitance idea with a conjecture that metabolic energy costs are an important constraint in terms of evolved function. The result is a much improved theory in terms of better matching with experimental measurements. Our simulations show that the metabolic energy associated with the velocity of the action potential attains a minimum near the biological values of ionic conductance density and axon diameter. This result appears to have little to no dependency on the temperature, axon model, or velocity considered, and thus strongly supports the energy-optimization conjecture.

The question of how physical and biological constraints have influenced the evolution of the nervous system has been an important question over the last decade. Biological sources of noise are often presumed to have a significant effect on information rates in neurons and presumed to influence the evolved coding strategies (Koch et al. 2004; Manwani and Koch 1999; Steinmetz et al. 2001). However, there are strong indications from the architecture of the brain that metabolic energy constraints have also played a major role (Laughlin and Sejnowski 2003; Sarpeshkar 1998). Levy and Baxter (1996) showed that the mean action potential frequency, which maximizes the information to energy ratio in certain coding schemes, is much smaller than the one that maximizes the information rate alone, and it is considerably closer to the mean frequencies actually observed. The maximization of energy efficiency also appears to obtain in the myelinated frog axon (Goldberg et al. 2003) and the salamander retina (Balasubramanian and Berry 2002). Furthermore, Levy and Baxter (2002) showed that quantal synaptic failures can also play a role in energy efficiency. Thus it is becoming clear that neural functioning, including neural codes, cannot be fully understood without an appreciation of the role of energy constraints.

TABLE 1. *Values of the fixed model parameters*

| Parameter | HH | HHSFL |
|---|---|---|
| $E_r$ (resting potential) | −65 mV | −65 mV |
| $E_{Na}$ (Na$^+$ equilibrium potential) | 50 mV | 50 mV |
| $E_K$ (K$^+$ equilibrium potential) | −77 mV | −77 mV |
| $m$ exponent in Na$^+$ channel model | 3 | 3 |
| $n$ exponent in K$^+$ channel model | 4 | 6 |
| $R_a$ (axoplasmic resistivity) | 35.4 $\Omega \cdot$ cm | 35.4 $\Omega \cdot$ cm |
| $R_o$ (extracellular resistivity) | 0 $\Omega \cdot$ cm | 0 $\Omega \cdot$ cm |
| $C_0$ (intrinsic membrane capacitance) | 0.88 $\mu$F/cm$^2$ | 0.88 $\mu$F/cm$^2$ |

Abbreviations refer to the axon models (see text). HH, Hodgkin–Huxley; HHSFL, Sangrey–Friesen–Levy.

METHODS

We used the NEURON and NMODL programming languages (Hines and Carnevale 1997) to develop computational models of the squid giant axon and wrote auxiliary codes in C to do parameter sweeps and minimizations; for these auxiliary codes, we incorporated routines from *Numerical Recipes in C* (Press et al. 1992). Our simulated axon was 10 cm long and divided into 1,000 isopotential segments, each of length 100 $\mu$m. The default axon diameter was 476 $\mu$m, although this was varied in our parameter sweeps. For numerical integrations, we used a second-order Crank–Nicholson method with a 1 $\mu$s time step. Tests with smaller axon segments and time steps significantly increased the computation time without noticeably changing the results.

For our main analysis, we used a reparameterized version of Hodgkin and Huxley's (HH) model of the squid giant axon. We also checked our major findings with the classic HH model. Details of these models are given below. Our models contained a voltage-independent leak conductance, which we divided into separate sodium and potassium leak conductances. They also contained voltage-activated sodium and potassium channels, along with a variable membrane capacitance that depended on the sodium channel gating current. The values of the biophysical parameters in the models are listed in Tables 1 and 2.

*Classic and reparameterized Hodgkin–Huxley channel models*

One of our axon models included the voltage-gated Na$^+$ and K$^+$ channel models proposed by Hodgkin and Huxley (1952) and the other used modified versions of the channels proposed recently by Sangrey, Friesen, and Levy (2004). We refer to these as the HH and HHSFL models, respectively. The reader may consult Hodgkin and Huxley, Sangrey et al., or a modern neuroscience textbook for details.

The equations given by Hodgkin and Huxley, which they obtained by fitting their action potential data in a way that, in a broad sense, agreed with their voltage-clamp data, are as follows.

- Active sodium conductance

$$g_{Na} = \bar{g}_{Na} m^3 h \quad (mS/cm^2) \tag{1}$$

- Sodium channel state variable equations

$$\frac{dm}{dt} = \alpha_m - (\alpha_m + \beta_m)m(t) \quad (ms^{-1}) \tag{2a}$$

$$\frac{dh}{dt} = \alpha_h - (\alpha_h + \beta_h)h(t) \quad (ms^{-1}) \tag{2b}$$

- Sodium channel activation and deactivation rates

$$\alpha_m(V_m) = \phi \times 0.1 \times \frac{-(V_m + 40)}{[e^{-(V_m+40)/10} - 1]} \quad (ms^{-1}) \tag{3a}$$

$$\beta_m(V_m) = \phi \times 4 \times e^{-(V_m+65)/18} \quad (ms^{-1}) \tag{3b}$$

- Sodium channel inactivation and deinactivation rates

$$\alpha_h(V_m) = \phi \times 0.07 \times e^{-(V_m+65)/20} \quad (ms^{-1}) \tag{4a}$$

$$\beta_h(V_m) = \phi \times \frac{b_{h1}}{\{e^{[-(V_m+65)+b_{h2}]/10} + 1\}} \quad (ms^{-1}) \tag{4b}$$

where $b_{h1} = 1$ ms$^{-1}$ and $b_{h2} = 30$ mV (these parameters are varied in the HHSFL model discussed in the following text).

- Temperature coefficient (which implies $Q_{10} = 3$)

$$\phi \equiv 3^{(T-6.3)/10} \tag{5}$$

- Active Na$^+$ current

$$I_{Na} = \bar{g}_{Na} m^3 h(V_m - E_{Na}) \quad (mA/cm^2) \tag{6}$$

- Potassium channel state variable equation

$$\frac{dn}{dt} = \alpha_n - (\alpha_n + \beta_n)n(t) \quad (ms^{-1}) \tag{7}$$

- Potassium channel activation and deactivation rates

$$\alpha_n(V_m) = \phi \times 0.01 \times \frac{-(V_m + 55)}{[e^{-(V_m+55)/10} - 1]} \quad (ms^{-1}) \tag{8a}$$

$$\beta_n(V_m) = \phi \times 0.125 \times e^{-(V_m+65)/80} \quad (ms^{-1}) \tag{8b}$$

- Active K$^+$ current

$$I_K = \bar{g}_K n^4 (V_m - E_K) \quad (mA/cm^2) \tag{9}$$

- Leak current

$$I_L = g_L(V_m - E_L) = g_{LK}(V_m - E_K) + g_{LNa}(V_m - E_{Na}) \quad (mA/cm^2) \tag{10}$$

- The Hodgkin–Huxley differential equation

$$\frac{d}{4R_a}\frac{d^2 V_m}{dx^2} = C_m(t)\frac{dV_m}{dt} + \bar{g}_{Na} m^3 h(V_m - E_{Na}) + \bar{g}_K n^4(V_m - E_K)$$
$$+ g_L(V_m - E_L) \tag{11}$$

We emphasize again that the channel rate coefficient *Eqs. 3a, 3b, 4a, 4b, 8a,* and *8b* are based on the 1952 experimental action potential and voltage-clamp measurements of Hodgkin and Huxley. Since that time, better experimental techniques, including those for measuring gating currents, have become available (e.g., Forster and Greeff 1990), and additional experiments have been published. It has become clear that the Hodgkin–Huxley model does not make use of two observed phenomena: the delay in the activation of the K$^+$ channel (the Cole–Moore shift) and the dependency of Na$^+$ inactivation on Na$^+$ activation rather than voltage. See Sangrey et al. (2004) for a summary of the shortcomings of the Hodgkin–Huxley model and references.

Sangrey et al. made modifications to the Hodgkin–Huxley channel model that improve the fit of the simulated action potential to the experimental data. In the HHSFL model, the exponent on $n$ in *Eq. 9* is increased from 4 to 6. This has the effect of increasing the potassium channel activation delay time. The sodium channel inactivation kinetics given in *Eq. 4b* are also changed: the parameter $b_{h1}$ is

TABLE 2. *Default values of the model parameters that were varied in sweeps*

| Parameter | HH | HHSFL |
|---|---|---|
| $g_L$ (leak conductance) | 0.3 mS/cm$^2$ | 0.3 mS/cm$^2$ |
| $\bar{g}_{Na}$ (maximum active Na$^+$ conductance) | 120 mS/cm$^2$ | 130 mS/cm$^2$ |
| $\bar{g}_K$ (maximum active K$^+$ conductance) | 36 mS/cm$^2$ | 36 mS/cm$^2$ |
| $C^{max}$ (maximum gating capacitance) | 0.13 $\mu$F/cm$^2$ | 0.13 $\mu$F/cm$^2$ |
| $d^g$ (axon diameter) | 476 $\mu$m | 476 $\mu$m |

The conductances and gating capacitance were always increased or decreased together by the same factor; the axonal diameter was varied independently.

increased from 1 to 1.8 ms$^{-1}$ and $b_{h2}$ is increased from 30 to 49 mV. The effect of this is to increase the inactivation rate by a factor of almost two at the peak of the action potential while suppressing it at the action potential foot; the action potential therefore rises farther and more quickly. The combined result of the changes is that the HHSFL action potential, shown in Fig. 1 (dashed curve), is a much improved fit to the experimental data during the rising phase and also for the first part of the falling phase. The other HHSFL model equations are the same as in the HH model. The results from our simulations of the HHSFL model suggest that the most accurate aspect of the HH model is the sodium activation, which Sangrey et al. did not change. The activation kinetics and associated gating currents are also primarily what determine our major results with respect to the energy of the action potential wavefront.

*Gating capacitance*

Hodgkin correctly ascertained that because the kinetics of the voltage-activated sodium and potassium ion channels are voltage dependent, charged components of the channels interact with electric fields. In the HH and HHSFL models, the gating particles carry this charge. The movements of the charges associated with a channel produce a small transient capacitance.

This current, known as the "gating" current, must be included on the right-hand side of *Eq. 11* because it contributes to the total current determining the behavior of $V_m$. (The gating current can have terms proportional to $dV_m/dt$, and therefore it can act like a capacitance.) The effective capacitance is then the sum of the intrinsic capacitance and the time-varying gating capacitance

$$C_m(t) = C_0 + C_g(t) \qquad (12)$$

The total capacitance used in the Hodgkin and Huxley model is 1.0 $\mu F/cm^2$. The intrinsic capacitance $C_0$ was measured to 0.9 $\mu F/cm^2$ (Gentet et al. 2000). The gating capacitance $C_g$ has a maximum value of about 0.15 $\mu F/cm^2$ and can vanish at its minimum (Fernandez et al. 1982). All of these experimental capacitance values have uncertainties of at least a few tens of nanofarads per square centimeter.

Following Adrian (1975) and Sangrey et al. (2004), we set the simulation values of $C_0$ to 0.88 $\mu F/cm^2$ and $C_g^{max}$ to 0.13 $\mu F/cm^2$, both of which are within the experimental limits. We also assumed
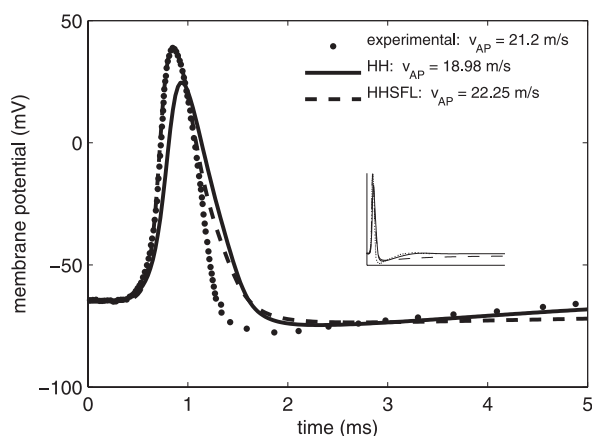


FIG. 1. Comparison of action potential models. Compared with the published 1952 action potential, the Sangrey–Friesen–Levy reparameterized Hodgkin–Huxley (HHSFL) action potential is the best fit for the initial rise on through to the peak and until the beginning of hyperpolarization, whereas the classic Hodgkin–Huxley (HH) action potential is too small in amplitude and too slow. In the late phase, the HHSFL model loses its advantage, but the differences are so small that they are irrelevant to the analysis here. All simulations and data are at 18.5°C using the published values for the conductances as listed in Table 2. *Inset*: when plotted over a longer (20 ms) time interval, the asymptotic return of the HHSFL action potential to rest is evident.

that the gating capacitance is linearly proportional to the number of closed sodium channels

$$C_g[m(t)] = \left(\frac{\bar{g}_{Na}}{g_{Na}^0}\right) \times [1 - m(t)] \times 0.13\,\mu F/cm^2 \qquad (13)$$

where $\bar{g}_{Na}^0$ is 120 mS/cm$^2$ for the HH model and 130 mS/cm$^2$ for the HHSFL model. Because the conductance ratio on the right-hand side of *Eq. 13* is fixed, increasing the density of sodium channels increases the gating capacitance proportionately.

If $C_g$ is interpreted as a true time-dependent capacitance, then the gating current also has a current component equal to $dC_g/dt \times V_m$, which should be added to the right-hand side of *Eq. 11*. We examined the effects of including this additional gating current component, and it is much smaller in magnitude than the $C_g \times dV_m/dt$ component. In terms of its effects on the ionic current fluxes, the data are changed by no more than about 5%. This change is to the overall normalization of the energy curve; its shape and the location of the minimum are unaltered. This effect is also considerably smaller than the effects of other experimental uncertainties on the ionic fluxes such as the overall gating capacitance (see RESULTS). Moreover, the gating capacitance is a phenomenological effect rather than a true additional capacitance and its exact behavior as a function of time is not well measured, which mitigates against using an overly detailed model of $C_g(t)$ in our simulations. Accordingly, the results reported here do not include the $dC_g/dt \times V_m$ component of the gating current.

The membrane capacitance per unit axial length is given by

$$C_m(t) = C_m(t) \times \pi d \qquad (14)$$

where $d$ is the axon diameter.

An alternate action potential, using Boltzmann kinetics at 5–8°C and modeling a space-clamped action potential (Clay 2005), fails to reproduce the traveling action potential at the relevant temperatures (unpublished observations).

*Temperature*

Most of our simulations were at 18.5°C, the same temperature at which Hodgkin and Huxley obtained their data for fitting the squid giant axon action potential. For both models we measured the action potential velocity as a function of temperature (Fig. 2) and, in addition, there were detailed parametrically varying simulations of the HHSFL axon performed at 12.5°C.

The temperature dependency of the HH and HHSFL models is contained in the $\phi$ factor (*Eq. 5*), which multiplies the rate parameters and implies a $Q_{10}$ value of 3 for all the rates. This factor was proposed by Hodgkin and Huxley as part of their empirical fit. Although we also included it, we note that this is not entirely rigorous: the usage of $\phi$ presupposes that the rates it multiplies are Boltzmann-like functions of energy, which $\alpha_m$ (*Eq. 3a*), $\beta_h$ (*Eq. 4b*), and $\alpha_n$ (*Eq. 8a*) clearly are not.

*Action potential stimulation and velocity*

We evoked an action potential by simulating a current injection into one end of the model axon. Generally, injections of about 10 $\mu A$ for 100 $\mu s$ were sufficient, although for some values of the biophysical parameters larger injections were necessary. After a brief initial phase, the properties of the resulting action potentials do not depend on the details of their production.

Simulated action potential velocities were determined from the times at which a particular polarization of the wavefront passed two different points along the model axon. We chose these points to be 5 and 8 cm from the simulated current injection site, by which time all the action potentials investigated had long since stabilized in shape and velocity.
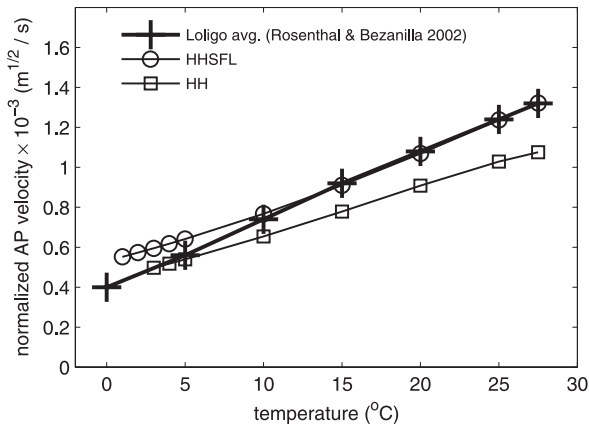
FIG. 2. Action potential velocities as functions of temperature. HHSFL model gives the best approximation to the experimental *Loligo* action potential velocities from 10 to 28°C. Below 8°C, the HH action potential model is a better fit. As in Rosenthal and Bezanilla (2002), all velocities are divided by the square roots of the respective axon diameters to normalize for different diameter values. Experimental data points (crosses) are an average of velocity measurements for 3 *Loligo* species taken by Rosenthal and Bezanilla (2002).

## Quantifying the energetic cost of current fluxes

Attwell and Laughlin (2001) estimated that roughly 75% of the total ATP consumed by the gray matter of rodent brain is used for communication and computation. In their Fig. 3*A*, they show their estimates of how this 75% is divided. The largest share of this ATP is associated with action potentials.

At 37°C the minimum free energy extracted from the ATP to adenosine diphosphate (ADP) that powers the $Na^+/K^+$ pump in heart is 50 kJ/mol (Jansen et al. 2003), and we used this value for the cost of ionic pumping in the squid axon at 18.5°C. Although the free energy has a different value at this temperature, it changes only the overall normalizations of the energy calculations below, but not the existence and locations of the energy minima; thus it does not alter the major conclusions of this study. Differences in pH can also affect the available free energy from ATP hydrolysis, but this, too, will change only the overall energy normalization.

During each cycle of the ionic pump, which consumes a single ATP molecule, three sodium ions are expelled from the neuron whereas two potassium ions are brought in. However, given that an axon always returns to its resting potential, over all time the integrated $Na^+$ and $K^+$ membrane fluxes are nearly equal so long as other fluxes are

much less. Because this assumption is consistent with Attwell and Laughlin's conclusion that most energy use goes to communication and computation, we thus assume that the third, i.e., extra $Na^+$ being pumped is used to power other membrane transport phenomena that are metabolically unavoidable. For example, the $Na^+$ gradient will be used to pump $Ca^{2+}$, glucose, acidic amino acids, and anions. Especially important are $CO_2$ and $H_2O$ in the form of $HCO_3^-$, whose buildup must be avoided but is the inevitable consequence of metabolism whenever ATP is consumed and regenerated through glucose or lactate. (Such a housekeeping role for the $Na^+/K^+$ pump has been pursued, even considered primary, by others, e.g., Stein 2002.) Thus given the 3:2:1 ratio of $Na^+/K^+/ATP$, it is our presumption that the number of ATP molecules required to restore the concentration gradients after an action potential is half of the total number of sodium ions that permeate the membrane during the action potential or, equivalently, half of the potassium ions that leave. The number of ions can, in turn, be calculated by integrating the ionic currents over an appropriate time interval. We chose this interval to be the 10 ms after the beginning of the action potential. As shown in the *inset* in Fig. 3, virtually all of the active ionic currents take place during the first 1 or 2 ms, and so the length of the integral is somewhat immaterial as long as it includes this initial period. We understand that not everyone agrees with the fate of the third $Na^+$ that is pumped per ATP (e.g., Attwell and Laughlin 2001). Fortunately, alternative formulations do not change the optimization results here. That is, one can rescale the energy consumed by a constant consistent with one's personal theory of the fate of the third $Na^+$.

Other sources of energy usage and loss are much smaller. During the HHSFL action potential, for example, the energy of Joule heating arising from the axial current is <3% of the net sodium flux energy and <1% of the total flux energy. We therefore neglect such effects.

## Variation of parameters

Parameter variation was performed in a way that kept the resting potential constant. With one exception, this amounted to scaling the voltage-dependent channel densities and leak conductance densities by a common factor. Thus we use one value, $\bar{g}_{Na}$, to represent all of these densities. The gating capacitance was also varied by this factor because it is proportional to the density of sodium channels. In the one exception, we tested the effects of varying only the leak conductance density. In this instance, only the single conductance $\bar{g}_L$ and the leak potential were changed, whereas all the other parameters were held fixed. The axonal diameter was varied independently.
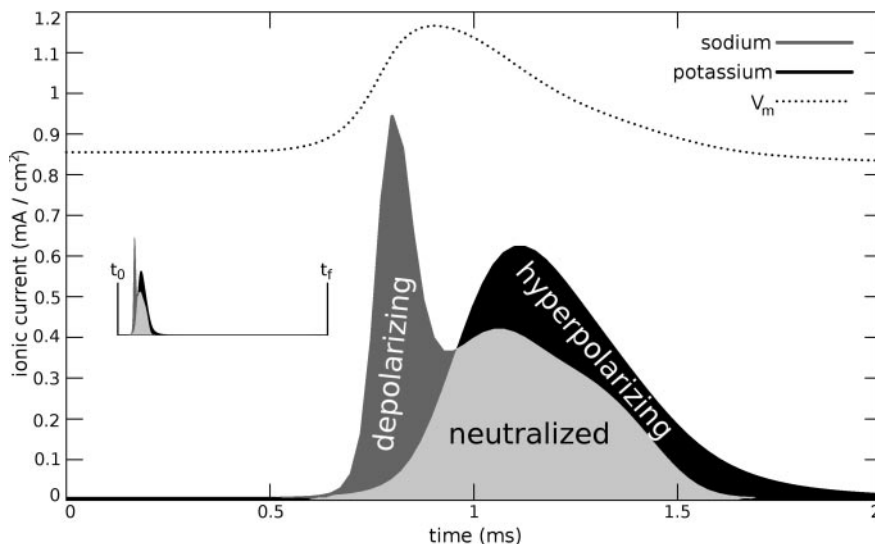


FIG. 3. $Na^+$ and $K^+$ currents during the action potential are naturally divided into 3 components: *1*) depolarizing net $Na^+$ current in the wavefront; *2*) net hyperpolarizing $K^+$ current just a little after peak depolarization; and *3*) neutralized currents that account for the overlapping and offsetting $Na^+$ and $K^+$ fluxes. HHSFL action potential is illustrated here. Total $Na^+$ current at any time is the sum of the depolarizing and neutralized currents and similarly for the $K^+$ current. Integral of each component (represented by the shaded areas in the figure) gives the associated flux, which is directly proportional to the energy used by the ionic pump to restore the resting concentration. *Inset*: temporally expanded plot, which begins at the foot of the action potential ($t_0$) and lasts for 10 ms ($t_f = t_0 + 10$ ms). Almost all of the ionic charge flux takes place during the first 1.5 ms.

## RESULTS

### Action potential simulations

The action potential produced by the Sangrey–Friesen–Levy reparameterization of the Hodgkin–Huxley squid giant axon model (HHSFL) gave a better fit to Hodgkin and Huxley's experimental data than the original Hodgkin–Huxley (HH) model did, as shown in Fig. 1. As discussed in METHODS, the chief differences between the two models are the $Na^+$ channel inactivation kinetics, as determined by the parameters $b_{h1}$ and $b_{h2}$ (Eq. 4b), and the $K^+$ channel delay, which, as suggested by Hodgkin and Sangrey et al. increased by changing the number of $K^+$ gating particles from four to six. The default model parameters (i.e., the published values listed in Tables 1 and 2) were used for all the simulations in this figure. The HHSFL model reproduces the rising phase of the action potential almost perfectly and it also reproduces the first half of the falling phase. The velocity of the simulated action potential is within about 1 m/s of the experimental value, notably closer than the classic Hodgkin–Huxley model.

In Fig. 1, the experimental (HH) and the HHSFL action potentials are aligned at the foot of each action potential. At the foot, the behavior of the membrane potential depends only on the passive characteristics of the axon and thus is model independent. Beginning from −65 mV, the rising phases of the experimental and HHSFL action potentials essentially coincide: the experimental action potential rises to its peak of +38.9 mV 0.592 ms after the foot, whereas the HHSFL action potential has a peak of +38.7 mV, which occurs 0.594 ms after the foot.

The two simulated action potentials then repolarize at different rates. The experimental action potential crosses −65 mV at 1.3 ms after the peak, reaching its maximum hyperpolarization of −77 mV at 1.261 ms after the peak. By comparison, the HHSFL action potential crosses below the −65-mV level 1.62 ms after its peak or some 320 $\mu$s later than the experimental action potential, then reaching its trough of −73.5 mV at 1.825 ms after the peak, which is 564 $\mu$s later than the experimental action potential trough.

The experimental and HHSFL action potentials also diverge in their final phases after the troughs: the experimental one experiences a small and slow second depolarization to −63.4 mV (i.e., 1.6 mV above rest) 6.158 ms after the peak and then returns quickly to rest. The HHSFL potential does not exhibit this kind of oscillation, but instead has a smooth and overly slow, asymptotic recovery from the trough.

By comparison to the HHSFL model or to the experimental data, the action potential produced by the HH model does not rise as quickly and its peak is about 15 mV lower than the experimental observation (Hodgkin and Huxley 1952). The HH action potential is quite similar, however, to the HHSFL action potential for the first few milliseconds after the peak; once at its trough, it returns to rest sooner than the HHSFL model and in this respect better reproduces the experimental data.

### Temperature effects

Recently, Rosenthal and Bezanilla (2000, 2002) measured the velocities of action potentials as functions of temperature in the giant axons of *Loligo* and *Sepioidea* squids. Figure 2 compares the action potential models to these data. The experimental velocities are averaged over the three *Loligo* species Rosenthal and Bezanilla studied, which at any given temperature and normalized for diameter, differ by at most about 0.1 on the vertical scale.

The experimentally based curve is approximately linear with respect to temperature and has a slope of 33.5 $m^{1/2} \cdot s^{-1} \cdot °C^{-1}$. For a 476-$\mu$m-diameter axon, the normalized velocities correspond to physical velocities of 17.3 and 21.2 m/s at 12.5 and 18.5°C, respectively.

Importantly, the HHSFL action potential velocities are essentially identical to the experimental velocities above 12°C and they constitute the better fit above 10°C.

At lower temperatures, particularly below about 8°C, the HH action potential velocities are closer than the HHSFL velocities to the experimental values. However, the lower temperatures at which the HH model gives better fits are not characteristic of the temperatures at which squid actually live, which is between about 10 and 20°C (Rosenthal and Bezanilla 2000).

### Current fluxes

Figure 3 shows the $Na^+$ and $K^+$ currents per unit membrane surface area as functions of time during an HHSFL action potential. Both currents are plotted as positive for purposes of comparison, although it should be remembered that they flow in opposite directions. The time integral of each current gives the total amount of $Na^+$ and $K^+$ ionic charge (more exactly, for Fig. 3, charge per unit area) crossing the membrane: this is equal to the area under each curve on the plot. These integrals are in turn directly proportional to the metabolic energy consumed because, as discussed in METHODS, the $Na^+/K^+$ pump must subsequently pump all of the ionic charge that crossed the membrane during the AP back in or out to restore the resting ionic concentration gradients.

An obvious feature of Fig. 3 is the substantial extent to which the $Na^+$ and $K^+$ currents "overlap." During much of the action potential, both currents are significant. Because $Na^+$ and $K^+$ ions each carry one unit of charge, a portion of the larger ionic current at a given time is balanced, or "neutralized," by the smaller one. Of the ions in the larger current, only those not neutralized by ions of the smaller, oppositely directed current flowing have any electrical effect. Thus it is solely this net or excess ionic charge that influences the membrane potential, and Fig. 3 is shaded to illustrate this.

The net $Na^+$ flux, which is responsible for the rising phase of the action potential, occurs first and is the dark gray region marked "depolarizing" in Fig. 3. The area of the dark gray region (i.e., its time integral) is the net, unbalanced sodium ion charge crossing into the membrane during the rising of the action potential; this area is directly proportional to the metabolic energy cost this depolarizing sodium charge incurs. Similarly, the net $K^+$ flux, which is the black region marked "hyperpolarizing" in the figures, is responsible for the falling phase of the action potential.

The first peak of the HHSFL $Na^+$ current in Fig. 3 occurs 100 $\mu$s before the peak of the action potential at a magnitude of 943 $\mu$A/cm$^2$ per unit axon surface area. The falling $Na^+$ current, at a value of 35 $\mu$A/cm$^2$, reaches equality with the rising potassium current 50 $\mu$s after the voltage peak, after

which it rises to a second peak of 417 $\mu$A/cm$^2$ at 150 $\mu$s after the action potential peak. From this second peak, the Na$^+$ current then declines over a period of about half a millisecond, approaching its rest value of 4 $\mu$A/cm$^2$. The decline is fairly steady, although there is a noticeable "hump" about halfway that is probably a slight overestimate of total Na$^+$ flux.

The period from the onset of the voltage-activated Na$^+$ current (slightly after the onset of the action potential) to the point of equality with the K$^+$ efflux is the period of the net inward, depolarizing Na$^+$ flux. In the HHSFL action potential, the total Na$^+$ influx over this period has a value of 0.108 $\mu$C/cm$^2$, which gives a flux per unit axon length of 16 nC/cm or an energy cost of 4.2 nJ/cm. Very late in the action potential, there is a very small secondary net Na$^+$ flux, although this is negligible compared with the other fluxes.

The K$^+$ current has only a single peak, which occurs 225 $\mu$s after the action potential peak at a magnitude of 0.621 mA/cm$^2$. It has a roughly Gaussian shape (SD $\approx$ 300 $\mu$s), although the curve, relative to a Gaussian, is slightly compressed on the front side. The net K$^+$ efflux begins at the equality of the Na$^+$ and K$^+$ currents and essentially continues for the rest of the action potential. The net K$^+$ flux has a value of 0.107 $\mu$C/cm$^2$, which is within 1% of the net Na$^+$ flux. The slight difference between the net fluxes is, we believe, explained by the fact that our gating capacitance approximation does not perfectly simulate the gating current and its contributions to the net Na$^+$ and K$^+$ fluxes, which in a fully accurate model would be equal. These contributions are very small in all the models we studied, however, and they do not significantly affect our conclusions; the resulting optimization properties (see following text) will apply for both net components. The associated energy cost of the net K$^+$ flux is 4.1 nJ/cm. (Of course the K$^+$ and Na$^+$ ions are pumped together; thus the costs of the K$^+$ and Na$^+$ fluxes are not to be added. See our assumptions in the METHODS section regarding the Na$^+$ and K$^+$ ratios and pumping.)

The currents in the HH action potential are qualitatively similar to those in the HHSFL model, although the peak of the K$^+$ current is almost as high as that of the Na$^+$ current in the older model, and significant quantitative error would follow in later energy calculations if we were to make do with the original 1952 model.

In terms of energy use, the most costly component in both models is the neutralized current, shown for the HHSFL model by the light gray shading in Fig. 3. In this region, the two currents completely negate each other; that is, the ionic fluxes have no influence on the action potential because there is no net movement of charge. Nevertheless, the ions of both species must be subsequently pumped back to restore their resting concentrations; thus the neutralized component also incurs an energy cost.

Of the two models, the HHSFL action potential has—both relatively and absolutely—the smallest neutralized current flux; the per length value is 32 nC/cm for each ion or, in energy units, 8.4 nJ/cm. Thus of the total action potential energy cost of 12.6 nJ/cm, fully two thirds is associated with charge movements that do not have any electrical effect. For the HH model, the percentage of metabolic costs resulting from these neutralized fluxes is even greater and, we believe, is overestimated.

Regardless of the model one prefers, it seems that the action potential is poorly designed and is wasting precious energy. However, as we shall speculate in the DISCUSSION, this cost may be unavoidable and evolvable but has nothing to do with velocity. Beyond such speculation, we can ask a more quantitative question: Is there any perspective that leads to an explicit efficiency in the action potential? To move in this direction, we study two easily evolvable biological parameters: $\bar{g}_{Na}$, the maximum active sodium conductance density, and $d$, the axon diameter.

*Action potential energy costs*

Spike velocity costs energy no matter how it is produced (Sangrey and Levy 2004); however, some mechanisms for producing it may be more economical than others. Here we study reparameterizations of isovelocity action potentials at 18.5 and at 12.5°C as a function of diameter and channel densities. To maintain the isovelocity constraint, we increase one parameter and decrease the other to produce new action potentials with the same velocity. Figure 4, a phase diagram, shows an isovelocity curve in conductance-diameter parameter space for the HHSFL model, where the velocity is within 0.01 m/s of the biological value (Hodgkin and Huxley 1952) of 21.2 m/s. Beginning at the *left* and moving to the *right*, the isovelocity curve starts where action potentials are reliable and falls from large-diameter values at low channel densities to a relatively flat region beginning at about 300 mS/cm$^2$, where the diameter value is about 380 $\mu$m. At higher conductances that are not shown in the figure, the diameter increases again to offset the substantial gating capacitance. The isovelocity curve for the HH model has similar features. In sum, such a phase diagram illustrates the boundary between faster action potentials (above the curve) versus slower action potentials (below the curve).

Figure 5 shows three of these isovelocity HHSFL action potentials. The larger-diameter and lower channel density action potentials rise more slowly and the peak heights are smaller. To compare energy costs of these different, but equal-velocity, action potentials, we quantify the Na$^+$ fluxes.

Both models produce a convex curve with a single minimum for the energy cost associated with the action potential wave-
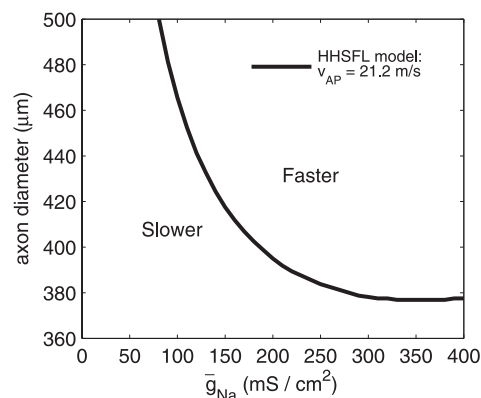


FIG. 4. Isovelocity curve (21.2 m/s) of the HHSFL model at 18.5°C. This phase diagram illustrates the trade-off between $\bar{g}_{Na}$ and diameter that produces a constant velocity of 21.2 m/s. Proportional variation of $\bar{g}_K$ and $g_L$ accompanies variation in $\bar{g}_{Na}$. Points on the isovelocity curve, which must be numerically computed, are all within 0.01 m/s (0.25%) of the experimental velocity and are in 10 mS/cm$^2$.
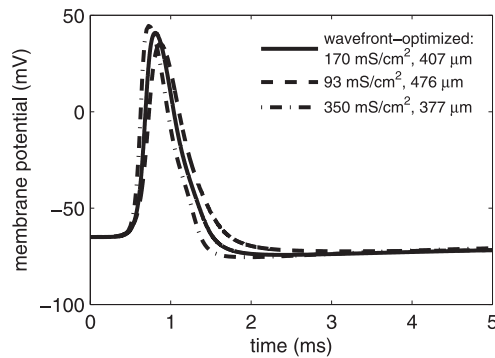
FIG. 5. Three different HHSFL action potentials on the 21.2 m/s isovelocity curve of Fig. 4. Solid curve indicates the action potential at the optimum of Fig. 6; a low-conductance ($\bar{g}_{Na}$ = 93 mS/cm², dashed curve) and a high-conductance ($\bar{g}_{Na}$ = 350 mS/cm², dash–dotted curve) action potential are also shown. Both greater amplitude and faster rise seem necessary when axon diameter is smaller.

front. For the HH and HHSFL models, these minima are near the measured values of conductance and diameter. Table 3 lists these minima and Fig. 6 shows the central result of this study.

The depolarization energies (solid symbols) and maximum membrane capacitances (open symbols) minimize near the biological values of ionic conductance and axon diameter and are approximately linearly related. The depolarization energy of the HHSFL model (Fig. 6, circles) has a minimum of 3.8 nJ/cm at $\bar{g}_{Na}$ = 170 mS/cm² and $d$ = 407 $\mu$m, but the precision of the minimum is tempered by the relative flatness of this curve between $\bar{g}_{Na}$ = 140 mS/cm², $d$ = 424 $\mu$m and $\bar{g}_{Na}$ = 220 mS/cm², $d$ = 389 $\mu$m.

The explanation for this minimum is related to the capacitance. The maximum HHSFL membrane capacitance per unit length, calculated according to *Eqs. 13* and *14* (with $m$ = 0, which is its approximate value at action potential initiation), is very similar in shape to the depolarization energy curve. It also has a relatively flat minimum, with the lowest point at $\bar{g}_{Na}$ = 180 mS/cm² and $d$ = 403 $\mu$m (although the variation from this point to $\bar{g}_{Na}$ = 200 mS/cm² is negligible). Because the depolarizing energy is directly proportional to the current going on to the membrane capacitance, this result reflects the fact that the depolarizing current during an action potential is used to charge the membrane capacitors. The HH isovelocity curve and its minimum are similar, although the diameters are larger than those for the HHSFL action potential.

Figure 6 also shows the depolarization energy and membrane capacitance curves for parametric variations of the 1952 Hodgkin–Huxley model (boxes). (As in the HHSFL curves, the low-conductance cutoff arises from the increasing difficulty of generating action potentials in this region.) Once again, the two curves have roughly the same shape, although they rise more steeply at high conductances than in the HHSFL model. The HH depolarization energy minimum of 5 nJ/cm occurs when $\bar{g}_{Na}$ = 160 mS/cm² and $d$ = 550 $\mu$m; as a function of the same

TABLE 3. *Depolarizing Na$^+$/minima*

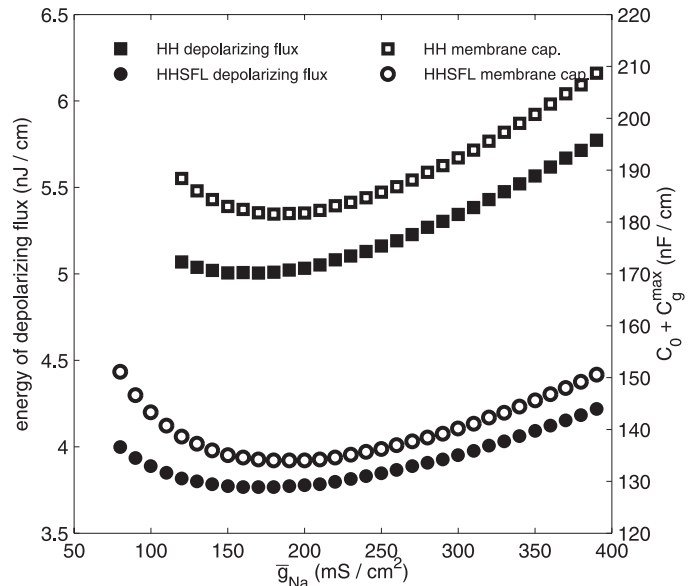| Model (Isovelocity) | Temperature °C | $\bar{g}_{Na}$, mS/cm² | $d$, $\mu$m | Metabolic Cost, nJ/cm |
|---|---|---|---|---|
| HHSFL (2004) (21.2 m/s) | 18.5 | 170 | 407 | 3.8 |
| HHSFL (2004) (17.3 m/s) | 12.5 | 160 | 410 | 3.8 |
| HH (1952) (21.2 m/s) | 18.5 | 160 | 550 | 5.0 |



FIG. 6. Minimum of the Na$^+$ depolarizing flux occurs near the biological conductance densities and near the minimum total capacitance. Minimization itself is similar for the HH and HHSFL models but the flux values are noticeably different, with the HH model producing a 30% overestimate of the depolarizing flux costs. Total capacitance and wavefront energetic costs are convex functions at isovelocity. Metabolic energy cost per unit length incurred by the net Na$^+$ current (solid symbols, *left axis*) and the total membrane capacitance per unit length (open symbols, *right axis*) are shown for the HH model (boxes) and HHSFL model (circles) at 18.5°C. All quantities are computed along the 21.2 m/s isovelocity curve for each model. Parametric dependency of the isovelocity curve for the HHSFL model is shown in Fig. 4; the isovelocity curve for the HH model has a similar shape. Similar minimizations of conductance density and capacitance, occurring near biological parameter values, are sensible because the membrane capacitance is what determines the energy that goes into generating the wavefront. Low-conductance cutoff of the curves is a result of the difficulty of generating action potentials in this region (it was possible to generate action potentials slightly further into this range for the HHSFL model). Overall energy normalization is derived as described in METHODS.

variables, the capacitance minimum occurs when $\bar{g}_{Na}$ = 180 mS/cm² and $d$ = 538 $\mu$m. The $\bar{g}_{Na}$ for minimal capacitance is the same as it is in the HHSFL axon, and the optimal $\bar{g}_{Na}$ for energy is only a few percent lower.

These optima are not only relatively independent of the model (i.e., HH or HHSFL) used, but they are also independent of the velocity used for the isovelocity curve and of the axon temperature. The HHSFL depolarization wavefront energy minima vary only by about 10 mS/cm² between the 15 and 25 m/s isovelocity curves, as do the capacitance minima (the small range of variation and the relative flatness around the minima make it difficult to identify the extent to which the variations in the depolarization and capacitance minima are correlated). At 12.5°C on the 17.3 m/s isovelocity curve, the HHSFL depolarization energy and capacitance minima occur when $\bar{g}_{Na}$ = 160 mS/cm² and $d$ = 410 $\mu$m. Thus at this lower end of the temperature range where squid generally live, the correspondence with the measured channel density is better. In this regard, the Hodgkin and Huxley (1952) value of 120 mS/cm² is of unknown accuracy and is arguably less precise than the Conti et al. (1975) value of 130 mS/cm². Indeed, there are suggestions that it could be even higher: Clay (2005) needed 180 mS/cm² to fit his sodium channel model to experimental data, which is from a space-clamped axon at low temperatures

(5–8°C) and is arguably more precise than space-clamped action potential data during the rising phase at higher temperatures. In sum, these optimal values for $\bar{g}_{Na}$ are within currently postulated ranges.

In addition to $\bar{g}_{Na}$, the measured membrane and gating capacitances are subject to error. Therefore we separately varied the intrinsic membrane capacitance between 0.88 and 0.9 $\mu$F/cm$^2$ and the gating capacitance between 0.13 and 0.15 $\mu$F/cm$^2$, which is roughly the range of experimental uncertainty in their values. We found that changing the intrinsic membrane capacitance had a relatively small effect. The gating capacitance also had a small effect on the capacitance minima, but a larger one on the energy minima, reducing the optimal sodium conductance densities by 20–40 mS/cm$^2$ as it was increased. That is, using 0.15 $\mu$F/cm$^2$, the value reported by Fernandez et al. (1982), implies the most energy efficient velocity when $\bar{g}_{Na}$ is 130 mS/cm$^2$. Thus there is little justification to go any further in our calculations until more precise measurements of both the gating capacitance and the sodium conductance density are produced.

The energy minima in Fig. 6 define a "wavefront-optimized" action potential for these models. Moreover, and as would be expected from Fig. 1, the wavefront-optimized action potential looks much the same as the default HHSFL action potential. The total energy cost of this optimized action potential is 13.4 nJ/cm, which is slightly higher than the default HHSFL model; however, the depolarization energy is about 10% lower.

The $y$-axis in Fig. 6 is expanded to make the energy minimizations more evident. Although the differences between the minimum energies and nearby points on the isovelocity curves are small with respect to the overall energy scale, we hypothesize that they could have been a significant factor in the evolution of the squid giant axon.

In contrast to the depolarization energy, we did not observe local minima in either the neutralized or total Na$^+$ flux energies, and this is true for both of the models studied. For example, in the HHSFL model, these energies increase fairly uniformly with channel density for the 21.2 m/s isovelocity curve, with a slope of about 35 pJ · cm · mS$^{-1}$.

We also investigated the effects of varying only the leak conductance $g_L$, which as noted we divided into separate voltage-independent sodium and potassium conductances. Increasing the leak conductance while maintaining the resting potential decreases action potential velocity. The relationship, up to about 17 times the experimental $g_L$ value of 0.3 mS/cm$^2$, is very nearly linear: increasing $g_L$ by 1 mS/cm$^2$ decreases the action potential velocity by 1.16 m/s. By contrast, the ion pumping energy associated with the leak channel increases linearly with $g_L$. Thus for reasons of both energetic cost and velocity, the leak should be as small as possible, although problems arise from the perspective of information transmission when it is <0.3 mS/cm$^2$. Specifically, the time to return to rest after an action potential lengthens significantly. Indeed, with a leak conductance density value of 0.1 mS/cm$^2$, the action potential does not return to rest in the time of the simulation. Thus further analysis of the role of $g_L$ is contingent on a better understanding of the information-theoretic properties of the axon. As noted previously, this is a large area of investigation requiring significant study in its own right.

## DISCUSSION

There are two primary findings here. First, the metabolic cost of the net initial Na$^+$ flux, or depolarization energy, minimizes near the biological values of ionic conductance density and axon diameter when the action potential is constrained to be at its experimentally observed value of 21.2 m/s. When other velocity values are used for this isovelocity constraint, the optimal axon diameter changes, but the optimal conductance densities do not. Thus so long as a constant velocity is used, the optimization of the conductance densities with respect to depolarization energy is independent of the chosen velocity.

The second important finding is that the largest component of the ion fluxes in the models studied is the neutralized flux, which incurs a metabolic energy cost just like the other components but has no effect on the membrane potential. The neutralized flux, in contrast to the depolarizing flux, does not show a minimum when the isovelocity constraint is imposed. Although Attwell and Laughlin (2001) correctly recognized the existence of overlapping currents, metabolic energy calculations that estimate the Na$^+$ influx during an action potential solely as the amount of charge placed on the membrane capacitor (i.e., the depolarizing flux) will be neglecting the majority of the metabolic cost. Even when the Na$^+$ influx estimated by depolarization energy is then multiplied by a constant factor to account for the neutralized Na$^+$ and K$^+$ currents, the correct functional relationship between the energy components and the diameter and conductance densities is not obtained.

Our division of the currents into the depolarizing, hyperpolarizing, and neutralized components, although artificial, is useful because it is easy, from a simulation perspective, to change the neutralized current without significantly affecting the net Na$^+$ and K$^+$ currents. This can be done by varying the K$^+$ conductance delay time, with longer delays producing less neutralized current (Sangrey et al. 2004 and unpublished simulations). In nature, the K$^+$ conductance delay appears to be an evolvable property, with different types of K$^+$ channels exhibiting a wide range of activation times (Coetzee et al. 1999). Given the diversity of K$^+$ channels, it is plausible that the K$^+$ conductance delay, like conductance density and axon diameter, is a parameter that evolution has optimized, although we believe that it relates to, and is in part constrained by, information transmission rates as well as energy. This is currently being investigated in detail.

The first result shows that Hodgkin (1975) and Adrian (1975) were on the right track in hypothesizing that the sodium channel gating current, which manifests as an additional, time-varying capacitance, plays an important role in optimizing the properties of the axon. What they were incorrect about was the quantity being optimized; specifically, they thought the velocity of the action potential, per se, was being optimized. The more accurate calculations of Sangrey et al. (2004) showed that this conjecture is unsatisfactory. The results described here suggest that it is, instead, the metabolic energy cost of the action potential velocity for which the conductance densities are optimized. That is, the combination of the sodium conductance density and the axon diameter lead to a minimization of the total membrane capacitance, and this total capacitance is

the primary property determining both the energy cost of the wavefront and the action potential velocity.

The models studied here, as well as by Sangrey et al. and Hodgkin and Adrian, are all of the squid giant axon. It is reasonable to wonder whether such findings can be generalized to the unmyelinated axons in mammalian neocortex, which dominate energy consumption by the brain (Attwell and Laughlin 2001). These axons operate at higher temperatures than the squid giant axon, can have different potassium ion channel types, are many times smaller, and have different action potential velocities.

To date, there have been no published direct measurements of the ion channel densities in unmyelinated neocortical axons, which have diameters several hundred times smaller than that of the squid giant axon and so are extremely difficult to voltage clamp. Two other invertebrate unmyelinated axons that have been investigated are the giant axons of *Myxicola* and crayfish. The sodium conductance density in *Myxicola* axons has been reported as about 46 mS/cm$^2$ (Bullock and Schauf 1978), which is well below our predicted optimal Na$^+$ conductance density of 170 mS/cm$^2$. However, other considerations make the relevance of this result to our study questionable. Inactivation in *Myxicola* Na$^+$ channels appears to be much more closely coupled with activation than it is in squid Na$^+$ channels, making the Hodgkin–Huxley assumption of independent activation and inactivation processes (which also is part of our simulations) inaccurate for this particular channel (Bell and Cook 1979; Goldman 1975). We have also been unable to find experimental measurements of propagating action potential velocities in *Myxicola* giant axons. In crayfish giant axons, the sodium channel density was inferred from gating current measurements (Starkus et al. 1981). Under certain assumptions about the conductance and gating charge per sodium channel (Hille 2001), the estimated crayfish $\bar{g}_{Na}$ is 1.2 to 1.7 times the squid axon value, which is within the range of our optimum. However, further experimental work on sodium conductance densities clearly is necessary for our conjecture to be decisively tested.

Because the total membrane capacitance is what determines the depolarization energy, the effects of these factors on the capacitance determine how generalizable our results are. For the reasons discussed in the following text, we believe that such a minimization is likely to occur in mammalian neocortical axons as well, provided that sodium activation and inactivation are not too strongly coupled (as in *Myxicola*).

The effects of increasing temperature are straightforward. The intrinsic (i.e., nongating) membrane capacitance, to a first approximation, is independent of temperature. The second-order error arises from differences in the distance between the polarized phosphate moieties of the inner and outer membrane leaves, which change only slightly with temperature.

The gating capacitance is determined by the motions of the S4 segments and the activation energy of the Na$^+$ channel. As it happens, molecular biology has confirmed that the S4 segments of the Na$^+$ channels are remarkably similar across species; thus the activation properties of the squid Na$^+$ channel differ little from those of any other Na$^+$ channel in axons that transmit information. This is likely explained by the fact that the S4 segment of the four subunits making up the membrane-spanning portion of the Na$^+$ channel protein have been highly conserved by evolution with respect to net moiety charge and

function. Moreover, as discussed in RESULTS, the capacitance minimum appears to be relatively independent of temperature in the 10–20°C range. Assuming that this is also true at higher temperatures and that effects such as charge separation, charge shielding, and potential focusing do not significantly alter the capacitance, we expect that the gating capacitance per Na$^+$ channel will be essentially the same in unmyelinated mammalian axons as it is in the squid giant axon.

The velocity independence of the conductance density optimization leads us to expect that, despite the different action potential velocities and smaller diameters of the mammalian neocortical axons, the sodium conductance densities will optimize around the same value. In this respect, the value of about 170 mS/cm$^2$ for $\bar{g}_{Na}$ may prove a universal constant for unmyelinated, signaling axons.

The isovelocity constraint used to obtain this optimization is itself a simplifying approach to an apparently intractable problem: What is the value of time? We originally tried to explicitly optimize time, but too many complexities resulted, including examples in which the value of time varied in a nonmonotonic fashion. For example, in muscular coordination, delivering information too soon can be just as much of a problem as delivering it too late. We concluded that if any immediate progress is to be made, assumptions should be adopted that avoid, or at least postpone, the problem of valuing time. As a result, we presume that evolution and development have produced the optimal axonal time delay in any given situation by producing the appropriate action potential velocity. In the event that the optimal time delay changes during development, the growing organism can adapt by changing the axonal diameter alone, not the sodium channel density.

Because of their large size, the neutralized currents, our second important result, demand attention and can be seen as a significant problem in their own right. The metabolic cost of these currents would, for instance, have a very substantial effect on the energy-optimal information rate as calculated by Levy and Baxter (1996). Although substantial work will be required to understand the relationship between the neutralized currents, the ion channel properties that determine them, and the information rates that result, our preliminary observations lead us to conjecture that the velocity of the action potential and the information rate can, to a large degree, be decoupled in an evolutionary and developmental sense and can thus be separately optimized. The large diversity of K$^+$ channels across species and cell types suggests that these may constitute the primary mechanism used by nature to determine information rates: in very slowly repolarizing pain fibers, for example, it has been argued that only a leak K$^+$ conductance is present, whereas in the owl auditory system Kv3.1 channels are highly expressed and seem to be responsible for the observed high-frequency firing (Parameshwaran et al. 2001). The different K$^+$ channels will lead to variation in the Na$^+$-K$^+$ current overlap and thus to differences in the costs of the neutralized currents. Future work will attempt to quantify these costs and discover any optimizations.

Finally, we offer a challenge to the molecular biophysicists. Combining the generality of our results with the highly conserved nature of the Na$^+$ channel in axons (Goldin 2002; Plummer and Meisler 1999) gives an explanation of the remarkable generality of the Hodgkin–Huxley results. Even without the results reported here, one could have presumed,

particularly for the S4 region of the Na$^+$ channels, which is the presumptive expression of the gating channels, that there is a molecular level optimization. The results here support the idea that it is reasonable to seek a quantifiable optimization of the charges on the S4 subunit played off against other aspects of Na$^+$ channel function that relate to the action potential velocity.

REFERENCES

**Adrian RH.** Conduction velocity and gating current in the squid giant axon. *Proc R Soc Lond B Biol Sci* 189: 81–86, 1975.

**Attwell D and Laughlin SB.** An energy budget for signaling in the grey matter of the brain. *J Cereb Blood Flow Metab* 21: 1133–1145, 2001.

**Balasubramanian V and Berry MJ II.** A test of metabolically efficient coding in the brain. *Network Comput Neural Syst* 13: 531–552, 2002.

**Bell J and Cook LP.** A model of the nerve action potential. *Math Biosci* 46: 11–36, 1979.

**Bullock JO and Schauf CL.** Combined voltage-clamp and dialysis of *Myxicola* axons: behaviour of membrane asymmetry currents. *J Physiol* 278: 309–324, 1978.

**Clay JR.** Axonal excitability revisited. *Prog Biophys Mol Biol* 88: 59–90, 2005.

**Coetzee WA, Amarillo Y, Chiu J, Chow A, Lau D, McCormack T, Morena H, Nadal MS, Ozaita A, Pountney D, Saganich M, Vega-Saenz de Miera E, and Rudy B**. Molecular diversity of K$^+$ channels. *Ann NY Acad Sci* 868: 233–285, 1999.

**Conti F, DeFelice LJ, and Wanke E.** Potassium and sodium ion current noise in the membrane of the squid giant axon. *J Physiol* 248: 45–82, 1975.

**Fernandez JM, Bezanilla F, and Taylor RE.** Distribution and kinetics of membrane dielectric polarization, II. Frequency domain studies of gating currents. *J Gen Physiol* 79: 41–67, 1982.

**Forster IC and Greeff NG.** High resolution recording of asymmetry currents from the squid giant axon: technical aspects of voltage clamp design. *J Neurosci Methods* 33: 185–205, 1990.

**Gentet LJ, Stuart GJ, and Clements JD.** Direct measurements of specific membrane capacitance in neurons. *Biophys J* 79: 314–320, 2000.

**Goldberg DH, Sripati AP, and Andreou AG.** Energy efficiency in a channel model for the spiking axon. *Neurocomputing* 52–54: 39–44, 2003.

**Goldin A.** Evolution of voltage-gated Na$^+$ channels. *J Exp Biol* 205: 575–584, 2002.

**Goldman L.** Quantitative description of the sodium conductance of the giant axon of *Myxicola* in terms of a generalized second-order variable. *Biophys J* 15: 119–136, 1975.

**Hille B.** *Ion Channels of Excitable Membranes* (3rd ed.). Sunderland, MA: Sinauer, chap. 12, 2001.

**Hines ML and Carnevale NT.** The NEURON simulation environment. *Neural Comput* 9: 1179–1209, 1997.

**Hodgkin AL.** The optimum density of sodium channels in an unmyelinated nerve. *Philos Trans R Soc Lond B Biol Sci* 270: 297–300, 1975.

**Hodgkin AL and Huxley AF.** A quantitative description of membrane current and its application to conduction and excitation in nerve. *J Physiol* 117: 500–544, 1952.

**Jansen MA, Shen H, Zhang L, Wolkowicz PE, and Balschi JA.** Energy requirements for the Na$^+$ gradient in the oxygenated isolated heart: effect of changing the free energy of ATP hydrolysis. *Am J Physiol Heart Circ Physiol* 285: H2437–H2445, 2003.

**Koch K, McLean J, Berry M, Sterling P, Balasubramanian V, and Freed MA.** Efficiency of information transmission by retinal ganglion cells. *Curr Biol* 14: 1523–1530, 2004.

**Laughlin SB and Sejnowski TJ.** Communication in neuronal networks. *Science* 301: 1870–1874, 2003.

**Levy WB and Baxter RA.** Energy efficient neural codes. *Neural Comput* 8: 531–543, 1996.

**Levy WB and Baxter RA.** Energy-efficient neuronal computation via quantal synaptic failures. *J Neurosci* 22: 4746–4755, 2002.

**Manwani A and Koch C.** Detecting and estimating signals in noisy cable structures, II. Information theoretical analysis. *Neural Comput* 11: 1831–1873, 1999.

**Parameshwaran S, Carr CE, and Perney TM.** Expression of the Kv3.1 potassium channel in the avian auditory brainstem. *J Neurosci* 21: 485–494, 2001.

**Plummer NW and Meisler MH.** Evolution and diversity of mammalian sodium channel genes. *Genomics* 57: 323–331, 1999.

**Press WH, Teukolsky SA, Vetterling WT, and Flannery BP.** *Numerical Recipes in C* (2nd ed.). Cambridge, UK: Cambridge Univ. Press, 1992.

**Rosenthal JJC and Bezanilla F.** Seasonal variation in conduction velocity of action potentials in squid giant axons. *Biol Bull* 199: 135–143, 2000.

**Rosenthal JJC and Bezanilla F.** A comparison of propagated action potentials from tropical and temperate squid axons: different durations and conduction velocities correlate with ionic conductance levels. *J Exp Biol* 205: 1819–1830, 2002.

**Sangrey T and Levy WB.** Conduction velocity costs energy. *Neurocomputing* 65–66: 907–913, 2005.

**Sangrey TD, Friesen WO, and Levy WB.** Analysis of the optimal channel density of the squid giant axon using a reparameterized Hodgkin–Huxley model. *J Neurophysiol* 91: 2541–2550, 2004.

**Sarpeshkar R.** Analog versus digital: extrapolating from electronics to neurobiology. *Neural Comput* 10: 1601–1638, 1998.

**Starkus JG, Fellmeth BD, and Rayner MD.** Gating currents in the intact crayfish giant axon. *Biophys J* 35: 521–533, 1981.

**Stein WD.** Cell volume homeostasis: ionic and nonionic mechanisms. *Int Rev Cytol* 215: 231–258, 2002.

**Steinmetz PN, Manwani A, and Koch C.** Variability and coding efficiency of noisy neural spike encoders. *BioSys* 62: 87–97, 2001.